

1-1-2007

Preparation and Characterization of Ordered TiO₂ Photocatalysts: Films and Mesoporous Structures

ORÇUN ERGÜN

OSMAN KARSLIOĞLU

AYŞEN YILMAZ

DENİZ ÜNER

Follow this and additional works at: <https://journals.tubitak.gov.tr/chem>

 Part of the [Chemistry Commons](#)

Recommended Citation

ERGÜN, ORÇUN; KARSLIOĞLU, OSMAN; YILMAZ, AYŞEN; and ÜNER, DENİZ (2007) "Preparation and Characterization of Ordered TiO₂ Photocatalysts: Films and Mesoporous Structures," *Turkish Journal of Chemistry*. Vol. 31: No. 5, Article 10. Available at: <https://journals.tubitak.gov.tr/chem/vol31/iss5/10>

This Article is brought to you for free and open access by TÜBİTAK Academic Journals. It has been accepted for inclusion in Turkish Journal of Chemistry by an authorized editor of TÜBİTAK Academic Journals. For more information, please contact academic.publications@tubitak.gov.tr.

Preparation and Characterization of Ordered TiO₂ Photocatalysts: Films and Mesoporous Structures

Orçun ERGÜN¹, Osman KARSLIOĞLU¹, Ayşen YILMAZ², Deniz ÜNER^{1*}

¹*Chemical Engineering Department, Middle East Technical University, 06531, Ankara-TURKEY*
e-mail: uner@metu.edu.tr

²*Chemistry Department, Middle East Technical University, 06531, Ankara-TURKEY*

Received 21.03.2007

Two different ordered TiO₂ structures were prepared as sol-gel films coated on glass and as mesoporous structures in order to study the effect, in 2-D or in 3-D, of bulk size on photocatalytic activity. Multilayer TiO₂ films were coated on glass by the sol-gel dip coating method. The UV-VIS characteristics of the films, with respect to the number of coating layers, were monitored. UV-VIS measurements implied an ordered TiO₂ structure grown on ITO glass. The second approach involved loading TiO₂ in mesoporous SBA-15 powder. Ti-SBA-15 with Ti/Si (mole/mole) ratios between 0.05 and 0.30 were prepared and characterized by XRD and BET. Low-angle XRD results of Ti-SBA-15 samples demonstrated long-range order, and the mesoporous structure of SBA-15 was preserved under all titanium loadings. Wide-angle XRD results of Ti-SBA-15 samples demonstrated no crystallinity for TiO₂ at low Ti loadings (0.05 and 0.10), and the onset of crystal formation at the 0.15 loading. The rutile phase was observed to be the dominant phase for lower loadings (0.20), whereas the anatase phase was dominant at higher loadings (0.25 and 0.30). BET surface areas decreased slightly with the addition of TiO₂ in SBA-15.

Introduction

Titanium dioxide (TiO₂) is used as a photocatalyst in such processes as industrial wastewater treatment, and the production of self-cleaning glasses and paints. Furthermore, it is used in dye-sensitized solar cells in which TiO₂ films are coated with Pt and dye sensitizers to convert solar light into electricity.¹ TiO₂ is a large-band-gap semiconductor with a catalytically active surface. Due to its band gap of 3.0-3.2 eV, it absorbs light in the UV range of the electromagnetic spectrum. Since UV light constitutes a small fraction of the incident solar radiation on the surface of the earth, extensive research has focused on increasing the activity of TiO₂ under visible light. This can be achieved by (i) inducing visible light activity to TiO₂, or (ii) by increasing the overall activity of TiO₂, such that its already visible light active portion is more effective.

Dye-sensitized solar cells, or Grätzel² cells, absorb visible light through dye sensitizers coated on the titania surface. The large scale use of organic dye sensitizers is hampered by their low thermal stability. Other approaches of inducing visible light activity to TiO₂ include introducing various elements (such as Pt,

*Corresponding author

Sn, Cu, Cr, Fe, W, N, S, and F) into the structure.²⁻⁸ These 2 methods differ in the process of modification of TiO₂ structures. In dye-sensitization, light harvesting molecules (LHM) that are adsorbed by TiO₂ mainly absorb light and transfer the charge to TiO₂, while dopants alter the bulk and surface states, and additional states are introduced, which allow absorption of visible light by the TiO₂ structures.

Regardless of the wavelength of the absorbed photons, increasing the photoactivity of TiO₂ should also increase its activity in the visible range of the spectrum. Since the photon absorption and the following reaction steps take place on the surface of TiO₂, the surface area of TiO₂ crystals is expected to have an important effect on photoactivity. For this reason, in order to increase photoactivity, titanium dioxide is loaded in high surface area mesoporous silica structure SBA-15, which has hexagonal pores 5-15 nm in diameter.⁹ Furthermore, increased surface area is not the only benefit of loading TiO₂ in SBA-15; quantum size effects,^{10,11} change in coordination number of titanium atoms¹², synergistic effects of the mixed oxides¹³ (SiO₂ and TiO₂), and mixed rutile-anatase phase¹⁴ also help increase photoactivity. By loading TiO₂ into SBA-15, it is expected that either titanium atoms are embedded into the silicate structure or they form crystallites in the pores of SBA-15. According to a model suggested by Tanabe et al.,¹⁵ direct substitution of silicon atoms in the SBA-15 framework with titanium atoms leads to tetrahedrally coordinated Ti atoms, which are known to be photocatalytically more active than octahedrally coordinated Ti atoms.¹² A modified version of this model was suggested by Liu et al.¹³ in which tetrahedrally coordinated Ti atoms are produced in the silicon-rich region of the mixed titania-silicate oxide. Therefore, according to this model, it is expected that the photoactivity increase due to a change in the coordination number of Ti atoms occurs at lower loadings of titania. At higher loadings, TiO₂ crystallites a few nanometers in size begin to form in the pores of SBA-15, where quantum-sized effects occur. Small crystallites of TiO₂ have a higher surface area to bulk ratio than that of the large TiO₂ crystals. Higher surface area results in an increase in the number of coordinatively unsaturated surface sites. It is known that in coordinatively unsaturated surface sites radiationless energy transfer occurs less efficiently than in saturated coordination sites;¹¹ therefore, small crystallites are expected to demonstrate higher activity due to less frequent recombination of electron-hole pairs by a radiationless energy transfer path. Lastly, crystals that have anatase and rutile phases of TiO₂ in contact have increased photoactivity due to a reduction in the rate of electron-hole recombination.

The objective of this work was to prepare and characterize ordered TiO₂ photocatalysts, either as films coated on glass or as mesoporous structures. These two different approaches will allow us study the effect in 2-D or 3-D of bulk size on photocatalytic activity.

Experimental Methods

Thin film TiO₂ preparation and characterization

TiO₂ films were coated on 2 types of glass substrates by the sol-gel dip coating method. The first type was ordinary flat window glass 30 × 50 × 3 mm, of unknown exact composition. The second type was flat ITO (Indium tin oxide) glass 25 × 50 × 2 mm.

Since the cleanliness of the substrate determines the quality of the film in this study, a surface cleaning procedure for ultra high vacuum parts was selected. For glass substrate cleaning, water, ethanol (96%), liquid detergent, and acetone (96%) were used. A solution of detergent-ethanol-water was prepared with an approximately 1:10:100 volumetric ratio. The substrates were put in the solution, which was then placed in a heated (about 50 °C) ultrasonic water bath and sonicated for 15 min. Finally, the substrates were rinsed

with water. This sonication-rinsing cycle was repeated 2 more times and the substrates were dried with a heating gun. The dried samples were sonicated in acetone for 10 min and rinsed with water. Finally, they were sonicated in ethanol for 10 min, rinsed with water, and dried with a heat gun. The samples were stored in similarly cleaned glass containers.

The sol was prepared from 180 mL of ethanol (99.9%, Merck), 9 mL of titanium isopropoxide (Ti(OCH(CH₃)₂)₄, 97%, Aldrich), 3.8 mL of acetic acid^a (99.9%, Fisher), and 1 mL of water. Water, ethanol, and acetic acid were mixed first, and titanium precursor was slowly added to the well-mixed solution in the final step. The mixture was stirred for 16 h in a sealed beaker with a magnetic stirrer. After this period, the solution was refrigerated for 3 days at 4 °C. Before coating, the sol was stirred until it reached room temperature. The coating was carried out at room temperature. Dipping was performed with a home-made electrically driven pulley system. Substrates were dipped in the sol at the rate of 10 cm/min, kept there for 10 min, and removed at the same rate. They were dried^b at 120 °C for 1 h. Then 2-layer and 3-layer coatings were prepared by repeating this procedure 2 and 3 times, respectively. Finally, all of the samples were calcined for 30 min at 400 °C and for 30 min at 500 °C. During coating the films on the flat substrates, the substrate was divided into 3 sections by masking the glass with plastic tape (Figure 1). Thus, it was possible to produce 3 stripes of coated areas of different thicknesses separated by uncoated zones after the removal of the mask. The masking tape was removed prior to calcination. It was not possible to remove all the organic residues remaining from the masking tape by calcination at 400 °C. Therefore, the samples were further calcined at 500 °C.

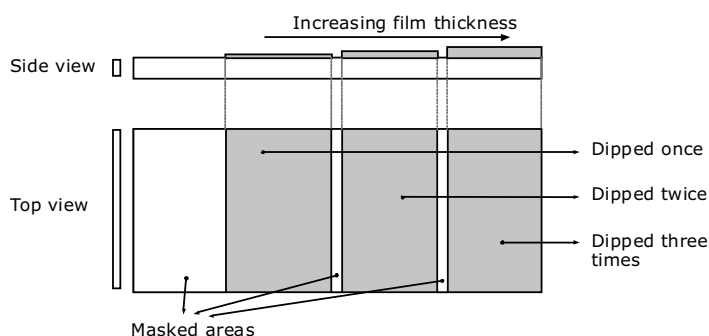


Figure 1. Film profile on flat glass.

The samples were characterized by transmission UV-VIS spectroscopy with a Varian spectrophotometer. UV-VIS spectra were recorded with respect to an uncoated clean glass of the same type as the reference. A baseline measurement was made with the uncoated glass as a sample and blank reference. X-ray diffraction measurements were performed with a Rigaku X-ray diffractometer with Cu target (30 kV, 15 mA). Film thickness measurements were carried out using a DekTak profilometer.

Ti-SBA-15 preparation and characterization

Distilled water (130 mL), containing 4 g of Pluronic 123 [poly(ethylene glycol) poly(propylene glycol) poly(ethylene glycol)] (Aldrich) and 19.5 mL of 1.5 M HCl was mixed for 1 h. Having acidic media adds long-range Coulombic interactions to the co-assembly process.⁹ After the polymer was fully dissolved in the

^aAcetic acid was preferred since it burns completely, leaving no residual ions after calcination.

^bDuring the drying and calcinations, the glass substrates were placed horizontally on glass boats.

acidic solution under vigorous mixing, 8.8 g of tetraethyl orthosilicate (TEOS), as the silicon source (98%, Merck), was added to the solution. At this step, titanium(IV) isopropoxide (Ti(OCH(CH₃)₂)₄ (98%, Acros Organics) of varying amounts was added to the solution to make different samples with Ti/Si ratios in the range of 0-0.30. At this stage, the solution was mixed for 24 h at 40 °C. It is very critical to keep the mixture at 40 °C because temperature differences more than 5 °C may damage the long-range order and mesoporous structure of the resulting structure. The solution was then put into Teflon bottles and aged in an oven at 90 °C for 24 h. This temperature was chosen as the temperature limit for aging because higher temperatures might boil water in the solution. The mixture was then filtered and air-dried for another 24 h. Calcination was carried out by slowly increasing the temperature from room temperature to 400 °C at 5 °C/min increments, kept at 400 °C for 1 h, and the temperature was then increased to 500 °C at a rate of 5 °C/min. Final calcination was carried out at 500 °C for 5 h.

X-ray diffraction measurements were performed with a Rigaku X-ray diffractometer with Cu target (30 kV, 15 mA). BET measurements were performed with a Micromeritics Gemini V-type surface and pore size analyzer.

Results and Discussion

Thin film TiO₂

TiO₂ films promoted with Pt and dye sensitizers were proven to be active under visible light irradiation for the reduction of CO₂ with H₂O.^{16,17} However, it was also observed in these studies that the response of the dye sensitizers to UV irradiation was different for thin and thick films. On thin films, sensitizers promoted UV activity, while on thick films they inhibited the reaction; therefore, it is very important to perform a detailed study on film thickness and its relationship to photoactivity. The films prepared as described in the experimental methods section were characterized for their film thickness and UV-VIS response.

Results of the film thickness measurements are given in Table 1. On both ordinary glass and ITO glass similar thicknesses were measured within the measurement sensitivity of the profilometer; therefore, only one value was reported. Film thickness increased nonlinearly with the coating of subsequent layers. There could have been several factors that affected the change in film thickness. One may have been the filling of pores, which are formed after drying, with sol and swelling of the sol during the subsequent drying. This hypothesis requires the formation of a highly porous coating, which is in fact consistent with the fluctuations in the thickness. Other than this, the increase in thickness in the subsequent layers could be attributed to the evaporation of the sol solvent during the waiting period in between the successive dipping processes. This increases the sol viscosity, which in turn results in a thicker film, according to the Landau-Levich equation.¹⁸

$$h = 0.94 \frac{(\eta \cdot v)^{2/3}}{\gamma_{LV}^{1/6} (\rho \cdot g)^{1/2}}$$

where h is the film thickness, η is the sol viscosity, v is the withdrawal speed, γ_{LV} is the liquid-vapor surface tension, ρ is the sol density, and g is the gravitational acceleration.

UV-VIS transmittance spectra for ordinary and ITO glass, which were dipped 1, 2, or 3 times^c, are given in Figures 2 and 3, respectively. On both samples, the absorbance increased with film thickness.

^cThe fluctuations around the 350 nm region are due to the instrument changing the light source from a tungsten to deuterium lamp and do not originate from the samples.

For films on ITO glass, there was a maximum absorption wavelength, while on ordinary glass no such maximum was observed. Maximum absorption was interpreted as an implication of an ordered structure, which probably resulted from the nucleation of TiO₂ on a highly ordered ITO surface, in comparison to the amorphous glass surface. The negative absorption in Figure 3 implies that reflection is important and

Table 1. Film thickness measurement results. The same thicknesses were achieved for both ITO and ordinary glass.

Number of times dipped	Film thickness
1	< 25 nm
2	~ 60 nm
3	~ 170 nm

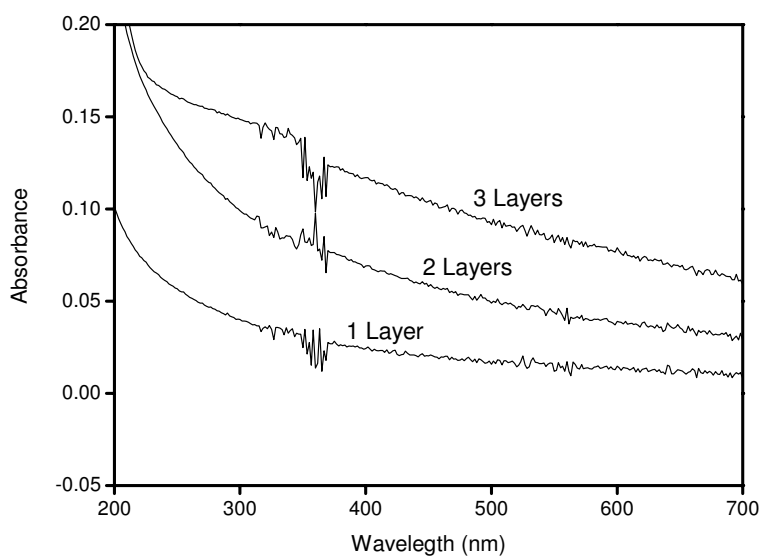


Figure 2. UV-VIS spectrum for TiO₂ film-coated ordinary glass dipped 1-3 times.

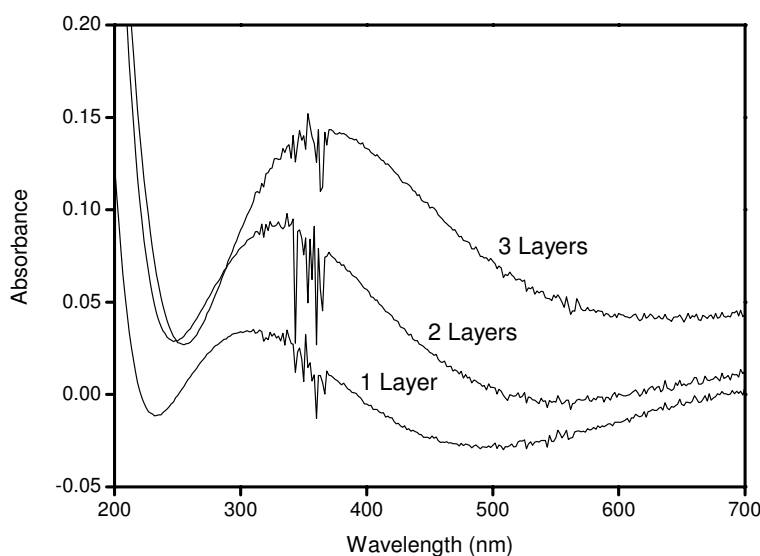


Figure 3. UV-VIS spectrum for TiO₂ film-coated ITO glass dipped 1-3 times.

indeed different for the ITO and TiO₂ coatings. XRD measurements did not yield any analyzable signal due to one or more of the following reasons: (i) the absence of short-range order. Although the films were thicker than 25 nm, it is possible that they were composed of smaller crystallites or amorphous structures. (ii) The sample amounts may not have been sufficient to obtain a reasonable S/N ratio for analysis. Therefore, it is difficult to comment on the crystallinity of these samples.

Ti-SBA-15

The Ti-SBA-15 samples were characterized for their BET surface areas and crystal structure via XRD. BET data given in Table 2 demonstrate that titanium loading into SBA-15 caused a slight decrease in the surface area of SBA-15. The area for 0.05 Ti/Si-loaded SBA-15 was an exception to this trend. This sample had a lower surface area than 0.10 Ti/Si-loaded SBA-15 did.

Table 2. BET surface areas and average adsorption pore sizes of Ti-SBA-15 structures at different loadings.

Ti/Si loading (mol/mol)	BET surface area (m ² /g)	BJH adsorption average pore diameter (Å)
0.00 ¹⁹	772.5	71
0.05	619	53
0.10	686	59
0.15	614	60
0.20	571	57
0.25	550	62
0.30	514	62

The two characteristic peaks of SBA-15 can be seen from the low-angle XRD measurements given in Figure 4. The data indicate that the Ti-SBA-15 structures were successfully synthesized, and long-range

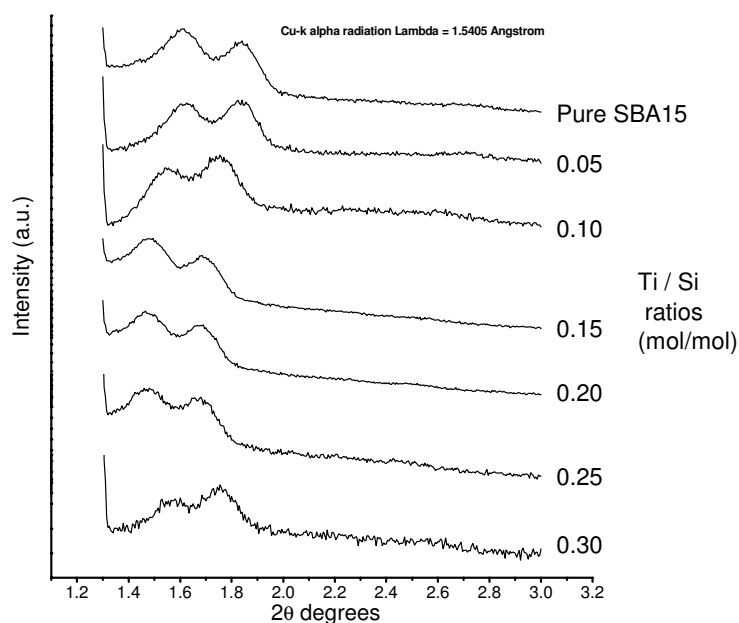


Figure 4. Low-angle XRD patterns of TiO₂-SBA-15 structures.

order and the mesoporous structure were preserved for all of the samples. High-angle XRD data, shown in Figure 5, demonstrate that no crystalline phase of TiO₂ was observed for 0.05 or 0.10 Ti/Si loadings. This may have been due to one or both of the following: titanium atoms are embedded into the SBA-15 structure and small crystallites that are not detectable by XRD are created. For Ti/Si loadings ≥ 0.15 , crystalline phases of TiO₂ were observed in the structure. The bold numbers above each peak in Figure 5 represent signal to noise ratios. When the signal to noise ratios are compared, it is seen that the rutile phase is the more abundant phase in the Ti-SBA-15 structure for the Ti/Si loading of 0.20. The anatase phase becomes the more abundant phase at higher loadings. Crystallite particles were between 10 and 20 nm, based on a preliminary calculation using Scherrer's equation. Further justification of particle sizes requires transmission electron microscopy measurements.

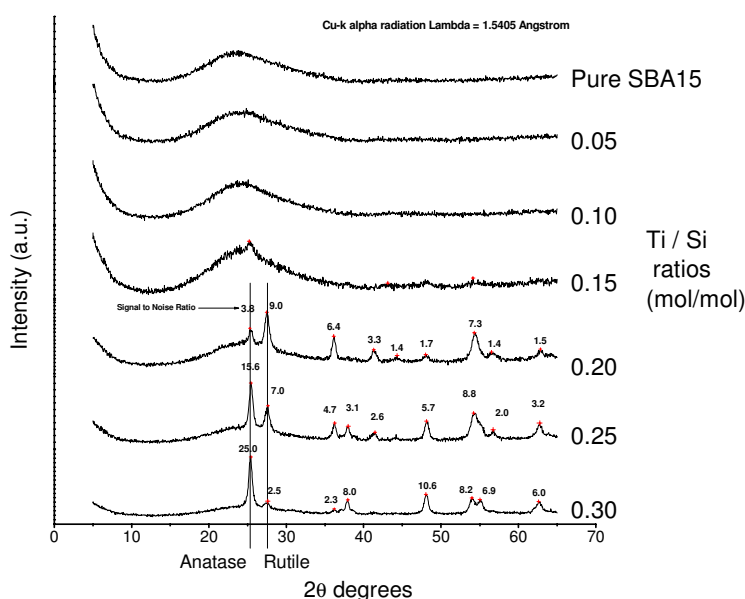


Figure 5. High-angle XRD patterns of TiO₂-SBA-15 structures.

Conclusions

In the first part of the study, thin films of TiO₂ were coated on flat ordinary and ITO glass, and ring-shaped borosilicate glasses via sol-gel dip coating. Measurement of film thickness by profilometry showed that films with thicknesses of ~ 25 , ~ 60 , and ~ 170 nm could be prepared. A nonlinear increase in film thickness with each additional layer of coating was attributed to swelling of the film during the drying process and the formation of a porous structure, and sol becoming more viscous due to solvent evaporation between each dip. XRD showed no crystallinity on the films; however, UV-VIS spectra gave the information of an ordered structure on ITO glass only.

In the second part, mesoporous SBA-15 structures loaded with TiO₂ were produced using direct sol-gel synthesis. Low-angle XRD analysis demonstrated that the long-range order and hexagonal mesoporous structure of SBA-15 were achieved and preserved under titanium loading. Wide-angle XRD analysis demonstrated that no crystalline phase was detectable for Ti/Si loadings of 0.05 and 0.10 m. At the loading of 0.15, crystallite formation was observed. Rutile is the more abundant phase for the loading of 0.20, while anatase is the more abundant phase at higher loadings. BET surface size analysis demonstrated that titanium loading

into SBA-15 caused a slight decrease in the surface area of SBA-15.

Acknowledgments

The authors would like to thank Professor Siddık İçli for the ITO glass, Bilkent University Physics Department for the film thickness measurements, and professors Engin Akkaya and Serdar Atılgan for UV-VIS measurements. This work was supported by TÜBİTAK under research grant no. ÇAYDAG 106Y075. O.K. and O.E kindly appreciate the graduate scholarships provided by TÜBİTAK BİDEB programs.

References

1. B. O'Regan and M. Grätzel, **Nature** **353**, 737-740 (1991).
2. M. Anpo and M. Takeuchi, **J. Catal.** **216**, 505-516 (2003).
3. M. Anpo, **B. Chem. Soc. Jpn.** **77**, 1427-1442 (2004).
4. D. Li, N. Ohashi, S. Hishita, T. Kolodiazhnyi and H. Haneda, **J. Solid State Chem.** **178**, 3293-3302 (2005).
5. D. Li, H. Haneda, S. Hishita, N. Ohashi and N.K. Labhsetwar, **J. Fluorine Chem.** **126**, 69-77 (2005).
6. R. Asahi, T. Morikawa, T. Ohwaki, K. Aoki and Y. Taga, **Science** **293**, 269-271 (2001).
7. M. Maeda and K. Hirota, **Appl. Catal., A Gen** **302**, 305-308 (2006).
8. W.-J. Chun, Y. Koike, K. Ijima, K. Fujikawa, H. Ashima, M. Nomura, Y. Iwasawa and K. Asakura, **Chem. Phys. Lett.** **433**, 345-349 (2007).
9. D.Y. Zhao, Q.S. Huo, J.L. Feng, B.F. Chmelka and G.D. Stucky, **J. Am. Chem. Soc.** **120**, 6024-6036 (1998).
10. M. Anpo, T. Shima, S. Kodama and Y. Kubokawa, **J. Phys. Chem.** **91**, 4305-4310 (1987).
11. M. Anpo, **Catal. Survey Jpn.** **1**, 169-179 (1997).
12. C. Beck, T. Mallat, T. Burgi and A. Baiker, **J. Catal.** **204**, 428- 439 (2001).
13. Z.F. Liu, J. Tabora and R.J. Davis, **J. Catal.** **149**, 117-126 (1994).
14. S. Bakardjieva, J. Subrt, V. Stengl, M.J. Dianez and M.J. Sayagues, **Appl. Catal., B Environ.** **58**, 193-202 (2005).
15. M. Itoh, H. Hattori and K. Tanabe., **J. Catal.** **35**, 225-231 (1974).
16. O. Ozcan, F. Yukruk, E.U. Akkaya and D. Uner, **Appl. Catal., B Environ.** **71**, 291-297 (2007).
17. O. Ozcan, F. Yukruk, E.U. Akkaya, D. Uner, **Top. Catal.**, **44**, 523-528 (2007).
18. L.D. Landau and B.G. Levich, **Acta Physiochim, U.R.S.S.** **17**, 42-54 (1942).
19. B. Akça, "Synthesis and Characterization of Co-Pb/SBA15 Mesoporous Catalysts" MS Thesis, Middle East Technical University, Ankara, Turkey, 2006.